The Contrasting Effects of Diethylmethylamine during Reduction of Protons and Oxidation of Formic Acid in Diethylmethylammonium-based Protic Ionic Liquids[§]

*Sean E. Goodwin,[1] Sayyar Muhammad,[2] and Darren A. Walsh[1,]**

[1] School of Chemistry and GSK Carbon Neutral Laboratory for Sustainable Chemistry

The University of Nottingham, Jubilee Campus

Nottingham NG7 2TU, UK

[2]Islamia College, Peshawar Khyber, Pakhtunkhwa

Pakistan 25120

* darren.walsh@nottingham.ac.uk; Tel: +44 115 8467495; Fax: +44 115 9513562

[§] Dedicated to the memory of Prof. Roger Parsons, F.R.S.C., F.R.S.

Abstract

Ionic liquids are formally defined as liquids that consist entirely of ions, and which are liquid below 100 °C. As these liquids are being proposed for use in a range of electrochemical devices and applications, understanding the electrochemical behaviour of these is increasingly important. In this contribution, we describe the effects of parent amine molecules on electrocatalysis in the protic ionic liquids diethylmethylammonium trifluoromethanesulfonate and diethylmethylammonium heptafluorobutanoate. We first show that diethylmethylamine can adsorb onto Pt electrodes during electrocatalytic reduction of trifluoromethanesulfonic acid in diethylmethylammonium trifluoromethanesulfonate. In contrast, diethylmethylamine promotes the oxidation of formic acid in this ionic liquid, by deprotonating the acid to the active formate species. Therefore, the neutral base can either inhibit or enhance electrocatalysis in the liquid, depending on the reaction under consideration. We also show that the mechanism of formic-acid oxidation in diethylmethylammonium heptafluorobutanoate differs significantly from that observed when using diethylmethylammonium trifluoromethanesulfonate. This phenomenon is attributed to adsorption of poisoning spectator species onto the electrode surface, demonstrating that changes to the structure of ionic-liquid anions can have drastic effects on the electrochemistry of these liquids.

Keywords: ionic liquid; ultramicroelectrode; scanning electrochemical microscopy; hydrogen evolution reaction; underpotential-deposited hydrogen; formic acid

1. Introduction

Ionic liquids are formally defined as materials that are composed entirely of ions and which are liquid below 100 °C [1]. Due to their inherent conductivities and thermal and electrochemical stabilities, ionic liquids are being used in an increasing number of electrochemical applications, including fundamental studies of the electrical double layer [2], investigations into mass and charge transport [3-4], electrochemical sensing [5], batteries [6], supercapacitors [7], and fuel cells [8]. While a large number of ionic liquids can potentially be synthesised, they can be broadly divided into two classes. Protic ionic liquids (PILs) are those formed by proton transfer from Brønsted acids to Brønsted bases, and aprotic ionic liquids are those formed by transferring any group other than a proton to the parent base [9].

Despite the fact that ionic liquids are defined as species that only contain ions, they can often behave as though they contain neutral species, exhibiting higher-than-expected vapour pressures and relatively-low conductivities. These phenomena are usually attributed to the presence of long-lived ion pairs or clusters, and neutral molecules, in the liquids [10-12]. Such effects are particularly common in PILs, which depending on the degree of proton transfer during synthesis, can comprise an equilibrium mixture of the salt, the parent base, and the parent acid:

$$\underset{\text{acid}}{HA} + \underset{\text{base}}{B} \leftrightarrows \overbrace{[BH]^+ + [A]^-}^{\text{salt}} \quad (1)$$

Non-stoichiometric PILs containing residual parent species can also form during the exothermic neutralisation reaction by loss of the most volatile component from the reaction mixture, unless very careful consideration is given to the reaction conditions [12-13].

Residual neutral molecules can have a significant effect on the electrochemical properties of ionic liquids. For example, water (a common contaminant in ionic liquids) can narrow their potential windows, reduce their viscosities, and increase the rate of mass transport to electrodes [14-16]. It was recently demonstrated that the electrochemical properties of non-stoichiometric PILs containing residual parent acids can differ significantly from those of the pure liquids. Electrochemical reduction of the residual acid in PILs at negative potentials yields H_2, and the potential at which O_2 is reduced depends on the acid content of the liquids [13]. However, to the best of our knowledge, no work has focussed on understanding the effects of parent bases on the electrochemical properties of PILs. Brønsted bases are often added in excess during synthesis of PILs [17], so it is important that any electrochemical effects due to residual bases in PILs are understood and can be identified.

In this contribution, we describe the use of proton reduction and formic acid (HCOOH) oxidation as model electrocatalytic reactions to probe the electrochemical behaviour of the PILs diethylmethylammonium trifluoromethanesulfonate, [dema][TfO], and diethylmethylammonium heptafluorobutanoate, [dema][HfB] (Scheme 1). We show that the parent amine diethylmethylamine (dema) adsorbs onto Pt ultramicroelectrodes (UMEs) during reduction of trifluoromethanesulfonic acid (TfOH) in [dema][TfO], poisoning electrocatalytic sites on the Pt surface. Conversely, HCOOH oxidation at Pt in [dema][TfO] is accelerated by addition of dema, due to the formation of the active species $HCOO^-$. In [dema][HfB], on the other hand, sluggish HCOOH oxidation is observed and the mechanism of $HCOO^-$ oxidation differs from that in [dema][TfO], an effect that is attributed to adsorption of $[HfB]^-$ ions onto the electrode surface. Therefore, our results show that parent amines, if present in ammonium-based PILs, can inhibit or enhance electrocatalytic reactions, depending on the reaction under study, while completely different behaviour can result from changing the structure of the PIL anions.

2. Experimental Section

2.1. Reagents and Apparatus

Electrochemical measurements were performed using a Model CH910 scanning electrochemical microscope and Model CH700 potentiostat (CH Instruments, Austin, TX). General chemicals were from Alfa Aesar or Sigma-Aldrich. H_2 (99.995 %), Ar (99.998 %), and N_2 (99.998 %) were from BOC gases (Nottingham, UK). Pt wire (0.5-mm diameter, 99.997%, and 0.025 mm diameter, 99.95%) and Pd wire (0.1 mm diameter, 99.99%) were from Alfa Aesar.

2.2 Synthesis of Ionic Liquids

[dema][HfB] and [dema][TfO] were prepared by adding aqueous 1.0 M heptafluorobutyric acid (HfBH) and 1.0 M (aq.) TfOH, respectively, to neat dema to a molar ratio of 1:1.05. The excess base was then removed under vacuum (2×10^{-2} mbar) at 70 °C over 48 hrs [13]. Non-stoichiometric [dema][TfO] containing 0.16 M excess TfOH (as measured using the method described in Reference [13]) was synthesised by addition of neat TfOH to dema. This PIL was also dried at 2×10^{-2} mbar and 70 °C for 48 hours. Residual water contents of all PILs were < 200 ppm.

2.3 Fabrication of Electrodes

25-μm and 50-μm diameter Pt UMEs were prepared by heat-sealing Pt microwires in borosilicate glass, exposing a Pt disk by grinding and polishing the glass, and making electrical

connections using Cu contact wires [18]. 25-μm diameter SECM tips were made using the same procedure, but the electrodes were sharpened until the ratio of the radius of the glass sheath to that of the Pt disk (the so-called *RG* value) was 3. 0.5-mm diameter Pt wires were used as counter electrodes. Pd/H reference electrodes, as introduced for use in PILs by Angell [17], were used in all electrochemical measurements, and were prepared by first annealing 0.1-mm diameter Pd wires in a butane flame. All potential are reported *vs*. Pd/H. The wires were then immersed in distilled water, and H_2 was bubbled over their surfaces for at least 30 min. The wires were then rinsed with deionised water, and dried under a flow of N_2. Electrochemical experiments were carried out at room temperature.

3. Results and Discussion

3.1 Effects of Diethylmethylamine on Proton Reduction at Pt in [dema][TfO]

We have recently shown that it is possible to quantify the concentration of precursor acids in PILs and to synthesise PILs that are effectively free of excess acid [13]. We begin by showing that even if a PIL contain excess acid, the parent base can persist and have an electrochemical effect in the PIL. Figure 1A shows the low-potential (low-*E*) region of cyclic voltammograms (CVs) of [dema][TfO] containing 0.16 M TfOH, recorded using a Pt UME. The cathodic process at $E < 0.0$ V is reduction of TfOH to H_2 (Equation 2) and, in the range $0.0 \text{ V} < E < 0.3$ V, adsorption and desorption of underpotential-deposited hydrogen, H_{upd}, occurs [19]. H_{upd} adsorption/desorption has only recently been observed in aprotic ionic liquids and PILs [20-22], and in the case of [dema][TfO] containing excess TfOH, occurs by reduction of TfOH (Equation 3). Note that in this potential region, only capacitive current flows at Pt in the pure

PIL [13]. Figure 1A shows that, as the upper potential limit of the voltammetric sweep increased, the charge under with the H_{upd} region increased (arrows).

$$Pt + 2TfOH + 2e^- \rightarrow Pt + H_2 + 2TfO^- \quad (2)$$

$$Pt + TfOH + e^- \leftrightarrows PtH + TfO^- \quad (3)$$

Figure 1B shows the H_{upd}-desorption charge (q) at each upper voltammetric potential limit, normalised by the H_{upd}-desorption charge recorded during voltammetry using the same Pt UME in aqueous 0.5 M H_2SO_4. The H_{upd}-desorption charge in aqueous 0.5 M H_2SO_4 was used as the normalisation factor, as a full monolayer of H_{upd} forms on Pt in this electrolyte, providing a measure the electrochemically-active (or real) surface area of Pt [23]. In all cases, the H_{upd}-desorption charge was significantly smaller in the PIL (<25 %) than in the aqueous electrolyte, and increased by more than a factor of 5 as the upper-potential limit increased from 1.2 V to 2.0 V. These observations indicate that some adsorbed species was blocking access of TfOH to active sites on the Pt surface (that is, significantly fewer Pt sites were available to form H_{upd} in the PIL), and that the poisoning species was removed at positive potentials.

To explore the poisoning of the Pt surface further, we used SECM, a technique that involves positioning a UME (which in SECM is called the tip) close to the surface of a second electrode (called the substrate). In the feedback mode of operation of SECM, steady-state electrolysis of a redox species occurs at the SECM tip, generating a steady-state tip current, i_T. If the tip is moved close to an insulating substrate, mass transport of the analyte to the tip is hindered, and the so-called 'feedback approach curve' shows a decrease in i_T as the tip-substrate distance, d, decreases. Conversely, if the electrolysed species can be regenerated at a conducting substrate, positive feedback occurs, and i_T increases as d decreases [24].

The black lines in Figure 2 show six consecutive SECM feedback approach curves recorded using an SECM tip immersed in [dema][TfO] containing 0.16 M TfOH, as the tip approached a Pt substrate. I_T is the tip current normalised by the steady-state tip current at (effectively) infinite distance from the substrate (that is, $I_T = i_T/i_{T,\infty}$), and L is tip-substrate distance normalised by the radius of the SECM tip (that is, $L = d/a$, where a is the radius of the SECM tip). In each case, the SECM tip was held at −0.7 V to drive the HER (Equation 2), and the Pt substrate was held at 0.4 V to drive oxidation of H_2, which yields protons that combine with the PIL anions to reform the parent TfOH (inset of Figure 2A) [17]. As L decreased, I_T increased due to positive feedback between the tip and the substrate. However, upon recording successive feedback approach curves (dashed and dotted lines), the curves shifted downwards, resulting in successive decreases in the maximum I_T at small L values. A control experiment was carried out by immersing a freshly-cleaned SECM tip in the PIL for 20 minutes (the same amount of time required to record all of the black curves), and then recording a feedback approach curve. Clearly, while a small decrease in the maximum I_T resulted when the tip and substrate were simply immersed in the PIL, the effects of recording consecutive feedback approach curves under potential control were much more significant.

To examine poisoning of the Pt surface further, SECM-tip CVs were recorded when the tip was held at various distances from an insulating substrate and the hydrogen evolution reaction (HER) was driven at the tip (Figure 3A). In each case the potential scan began at –0.8 V and the positive-potential limit was 1.5 V. When the tip was held at d = 60 μm, the steady-state HER current was about 30 nA and was slightly smaller during the positive sweep than during the negative sweep. As d decreased, the steady-state HER currents decreased significantly, as expected for hindered diffusion of TfOH to the tip surface. However, the steady-state current was significantly higher during the negative sweep than during the initial, positive sweep. When the tip was held at d = 25 μm (L = 2) and d = 15 μm (L = 1.2), the HER

currents during the negative sweeps were about 23 nA and 12 nA, respectively. These currents are about 75% and 40% of the steady-state current at d = 60 μm (L = 4.8), which is expected when hindered diffusion of TfOH to the tip occurs (that is, when pure negative feedback occurs) [25]. However, the significantly smaller tip currents that flowed during the positive sweeps when the tip was held close to the substrate indicates that trapping of the poisoning species in the tip-substrate gap causes significant poisoning of the electrode. However, this poisoning can be mitigated by executing the positive-potential excursion.

Finally, the SECM tip was held at d = 25 μm and successive CVs were recorded as the upper potential limit was increased from −0.5 V to 0.2 V, while keeping the initial potential at −0.8 V (Figure 3B). When the positive-potential limit was −0.5 V, the HER current was about 3 nA, and it overlapped in the positive and negative sweeps. As the upper potential increased, the HER current during the positive sweep remained at about 3 nA, but the HER current during the negative sweep increased (as indicated by the arrows in the figure). When the upper-potential limit increased to about −0.2 V, the negative sweeps started to show a peak-shaped current response during the negative sweep, which increased in magnitude as the positive-potential limit increased. The reason for the increasing current during the negative sweep is the rate of the HER started to increase due to the successive cleaning of the electrode, but this was countered by poisoning of the electrode, yielding the peak. Notably, when the most positive upper potential limit (0.2 V) was used, a marked increase in the HER activity of the Pt electrode occurred, and a steady-state HER current of about 23 nA flowed.

We consider now the identity of the poisoning species that persists in [dema][TfO] and poisons the Pt surface during H_{upd} adsorption and the HER. That H_{upd} adsorption was hindered in the liquid (Figure 1) indicates that the poisoning species was in the as-synthesised PIL. However, the HER was exacerbated by holding the electrode at negative potentials (Figures 2 and 3). The major species in the PIL were $[dema]^+$ cations, $[TfO]^-$ anions, TfOH, H_2 generated

at negative potentials, and possibly some dema that persists in the PIL at its equilibrium concentration. First, it is unlikely that the adsorbed species was $[TfO]^-$, as one would expect $[TfO]^-$ to become more strongly adsorbed at more positive potentials. It has also been shown that $[TfO]^-$ does not adsorb onto Pt surfaces from aqueous solution [26]. The exacerbation of the poisoning when the electrode was held at negative potentials to drive the HER indicates that the poisoning species was not $[dema]^+$, which existed at a high concentration prior to electrolysis. H_2 appears to be readily oxidised at Pt in this PIL [8], meaning that it is also unlikely that H_2 is responsible for the effect.

The final species that may be responsible for poisoning of the electrode is dema. Consideration of Equations 2 and 1 indicates that consumption of TfOH at the electrode surface to generate $[TfO]^-$ anions would cause a shift in the equilibrium generating dema, meaning that the parent base is likely responsible for the effect (the greatest poisoning effects are observed when TfOH is consumed). Note that it is not possible to test this hypothesis by simply adding excess dema to the PIL and examining its effect on H_{upd} deposition. The reason for this is that adding dema has the effect of neutralising the TfOH probe, making it difficult to observe H_{upd} deposition. In addition, changing the concentration of TfOH also affects the onset potential of the HER, making comparisons of the H_{upd} region difficult. Instead, as we have shown here, H_{upd} adsorption/desorption and the HER can be used as probe reactions into the effects of the dema that persists at equilibrium. That dema is responsible for the electrode poisoning is supported by the data in Figure 1A. At 0.2 V, complete H_{upd} desorption occurs, liberating protons from the electrode. These protons can then react with adsorbed dema to form $[dema]^+$, which does not hinder the HER.

3.2 Role of Diethylmethylamine during Oxidation of Formic Acid in [dema][TfO]

In this section, we show that dema has a very different effect on electrocatalysis of HCOOH oxidation than on TfOH reduction in PILs. However, before describing HCOOH electrooxidation in PILs, we briefly describe HCOOH oxidation in aqueous acidic media, to act as a reference for our discussion of HCOOH electrochemistry in PILs. Figure 4 shows CVs of 0.5 M H_2SO_4 in the presence (dashed line) and absence (solid line) of 0.5 M HCOOH using a Pt electrode. In blank H_2SO_4, typical H_{upd} adsorption/desorption and oxide adsorption/desorption features are visible between 0.0-0.3 V and 0.8-1.2 V, respectively. In the presence of HCOOH, oxidation of HCOOH resulted in peaks at about 0.3 V and 0.9 V in the forward sweep, and a second oxidation wave appeared at about 0.5 V during the negative sweep. This response is consistent with the accepted dual-pathway mechanism of HCOOH oxidation in aqueous electrolytes, in which direct HCOOH oxidation to CO_2 is accompanied by a pathway involving an adsorbed CO (CO_{ads}) intermediate. The CO_{ads} intermediate is oxidised near 0.9 V, coinciding with the formation of oxide groups on the surface of the Pt [27]. During the reverse (negative) sweep, the Pt-oxide layer is reduced, leaving a surface free from both oxides and CO_{ads}, and resulting in the large oxidation peak centred at about 0.5 V [28].

Figure 5 shows CVs of [dema][TfO] recorded using the same Pt electrode as used to record the CVs shown in Figure 4. In the absence of HCOOH (solid line), a low background current flowed. Some Pt oxides form positive of about 1.0 V in this liquid due to oxidation of trace water in the PIL [21,29]. The CV recorded in the PIL containing HCOOH (dashed line), is similar to that recorded when using the aqueous electrolyte. An oxidation current flowed at E >0.0 V, due to direct oxidation of HCOOH at the Pt surface. As the potential increased above about 1.0 V, the oxidation current increased significantly, coinciding with the formation of oxides on the Pt surface. During the negative sweep, the anodic current decreased as E decreased below 1.0 V, and a large peak that centred about E = 0.4 V appeared as surface

adsorbates were removed from the surface. Oxidation of HCOOH in [dema][TfO] then appears to follow similar behaviour to the oxidation in aqueous electrolytes; direct HCOOH oxidation occurs at low potentials and indirect oxidation occurs at high potentials, before the surface is cleaned of poisoning CO_{ads}-type species during the negative sweep and HCOOH oxidation resumes.

There has been considerable discussion in the literature on nature of the active species during HCOOH oxidation in aqueous media. Since its spectroscopic identification by Osawa [30], the involvement of an adsorbed formate, $HCOO_{ads}$, species during HCOOH oxidation has been the subject of some debate [31-32]. Recent data showing a clear increase in the rate of HCOOH oxidation as the pH of the electrolyte increases supports the involvement of $HCOO^-$ as an active species [32-35]. The mechanism of HCOOH oxidation in [dema][TfO] was examined by adding increasing amounts of dema to the HCOOH-containing PIL and recording CVs after each addition (Figure 6). In each case the reverse peak is shown to highlight the HCOOH-oxidation peak on the Pt surface after removal of the posisoning CO_{ads} species, as done by Joo and co-workers [32]. The peak current for HCOOH oxidation increased as the concentration of dema in the electrolyte was successively increased from 0.0 M (black line) to 0.3 M (red line), 0.5 M (green line), and 0.8 M (blue line). 0.1 M TfOH was then added to the PIL and the pink line in Figure 6 shows the resulting response. Upon acidification of the PIL, the HCOOH-oxidation current decreased again, as the effects of the added base were neutralised. Therefore, it appears that the added dema (pK_a in aqueous media = 10) deprotonated HCOOH (pK_a in aqueous media = 3.75), yielding $HCOO^-$ which was the active species. Note that the use of aqueous pK_a values as an indicator of the driving force for proton transfer in ionic media has been used previously, particularly as a qualitative estimate of ionicity in PILs [36]. However, it has been shown that the effective pK_as of amines in ionic liquids are sensitive to the structure of the amines, complicating their use [37]. There have

been some recent efforts towards determining pK_a scales in ionic liquids [38-39]. The data here suggest that the electrooxidation of HCOOH could be used as an electrochemical method to determine relative pK_as in ionic liquids and this is being pursued in our laboratories.

3.2 Oxidation of Formic Acid in [dema][HfB]

Figure 7 shows CVs of [dema][HfB] in the absence (dashed line) and presence (solid line) of 0.5 M HCOOH. It is clear from these data that oxidation of HCOOH in [dema][HfB] is different to that observed in [dema][TfO]. An HCOOH-oxidation current did flow at $E > 0.0$ V due to direct oxidation of HCOOH at the Pt surface (see inset of Figure 7 for a magnified view of the low-E region). However, the magnitude of the direct HCOOH-oxidation current is smaller than observed using [dema][TfO]. A larger HCOOH-oxidation current began to flow at about 0.9 V, coinciding with the onset of oxidation of the Pt surface, suggesting that some HCOOH oxidation proceeded via a CO_{ads}-type intermediate. However, unlike in [dema][TfO] and aqueous media, no significant HCOOH-oxidation peak appeared during the negative sweep. We ascribe this change in mechanism of HCOOH oxidation to adsorption of spectator ions, which block active sites for HCOOH adsorption, onto the Pt surface in [dema][HfB]. As $[dema]^+$ is present in both liquids, it appears that $[HfB]^-$ ions hindered HCOOH oxidation.

The effects of added base on HCOOH oxidation in [dema][HfB] were determined by adding dema and then TfOH to the PIL. Figure 8 shows a linear-sweep voltammogram of [dema][HfB] containing 0.5 M HCOOH (solid line). This response is compared with that recorded after adding 60 mM HfBH (dotted line), and 120 mM dema (dashed line) to the PIL. As observed when using [dema][TfO], addition of acid hindered HCOOH-oxidation via the direct route, and addition of excess dema increased the anodic current at low potentials, meaning that HCOOH oxidation at low potentials in [dema][HfB] probably also proceeds via

$HCOO^-$. This similarity notwithstanding, comparison of HCOOH electrooxidation in [dema][TfO] and [dema][HfB] reveals that changes to the anion structure can result in significant changes to their electrochemical behaviour.

4. Conclusions

We have shown here that it is possible to observe the electrochemical effects of parent amines in protic ionic liquids using electrocatalytic reactions as probes. On one hand, the amine diethylmethylamine suppresses H_{upd} adsorption/desorption onto Pt from the [dema][TfO] by co-adsorbing onto the Pt surface. However, adsorption is not irreversible, and the poison can be partially removed by sweeping the electrode to highly-positive potentials. On the other hand, diethylmethylamine enhances HCOOH oxidation, by deprotonating HCOOH, demonstrating that HCOOH oxidation proceeds *via* a formate intermediate in the PIL. These observations illustrate the contrasting roles that the amine can play during electrocatalysis in PILs. In addition, we showed that anion adsorption appears to hinder oxidation of HCOOH in [dema][HfB]. Therefore, when using protic ionic liquids for electrochemical applications, one should always consider the effects of any unreacted parent reagents in the liquid. In addition, strong adsorption of ions onto electrode surfaces from PILs can affect the electrochemical behaviour of these liquids and one should also consider such phenomena when using these liquids as electrolytes.

Acknowledgements

We thank the Engineering and Physical Sciences Research Council for funding through the Fuel Cells and their Fuels Centre for Doctoral Training (Project EP/L015749/1) and through Project EP/P002382/1.

Figure Legends

Figure 1. (A) Cyclic voltammograms of [dema][TfO] containing 0.16 M TfOH recorded using a 25-μm diameter Pt UME. Potentials were swept at 50 mV s^{-1} between −0.3 V and increasingly-positive upper potential limit (from 1.2 to 2.2 V) and the currents increased as the positive limit increased. (B) Graph of the H_{upd}-desorption charge, q, as a function of the upper potential limit during cyclic voltammetry. Charges are divided by the H_{upd}-desorption charge recorded using the same electrode in 0.5 M H_2SO_4.

Figure 2. (A) Consecutive SECM approach curves recorded using a 25-μm diameter Pt SECM tip polarised at −0.8 V, as it approached a 2-mm diameter Pt-disk substrate held at 0.4 V at an approach speed of 1 μm s^{-1}. The electrolyte was [dema][TfO] containing 0.16 M TfOH. The maximum I_T value decreased during successive experiments. The blue curve was recorded using a cleaned SECM tip that had been immersed in the liquid for 20 minutes. The inset is a schematic showing positive feedback of the redox species to the SECM tip.

Figure 3. (A) Negative-feedback mode SECM tip cyclic voltammograms recorded using the experimental setup described in Figure 2, but while the SECM tip was stationary. The tip potential was cycled between −0.8 V (initial potential) and 1.5 V at 50 mV s^{-1}, while the tip was held at various distances from an insulating (PTFE) substrate. (B) Successive negative-

feedback mode SECM tip cyclic voltammograms recorded at 50 mV s^{-1} at a tip-insulating substrate distance of 25 μm. The negative-potential limit was −0.8 V and the initial potential increased from −0.5 V, to −0.4 V, −0.3 V, −0.2 V, −0.1 V, 0.0 V, 0.1 V, and 0.2 V, leading to higher HER currents (as shown by the arrows).

Figure 4. Cyclic voltammograms of Ar-saturated 0.5 M H_2SO_4, recorded using a 50-μm diameter Pt UME at 50 mV s^{-1}. The applied potential was swept between −0.05 V (initial potential) and 1.4 V. The solid line shows voltammogram recorded in the absence of HCOOH, and the dashed line shows that recorded after addition of 0.5 M HCOOH.

Figure 5. Cyclic voltammograms of Ar-saturated [dema][TfO], recorded using a 50-μm diameter Pt UME at 50 mV s^{-1}. The potential was swept between 0.0 V (initial potential) and 1.6 V. The solid lines show voltammogram recorded in the absence of HCOOH, and the dashed lines show that recorded after addition of 0.5 M HCOOH.

Figure 6. Linear sweep voltammograms of Ar-saturated [dema][TfO] containing 0.5 M HCOOH, recorded using a 50-μm diameter Pt UME at 50 mV s^{-1} by sweeping the potential from 1.8 V to 0.0 V. Voltammograms were recorded after in [dema][TfO] containing (black line) 0.5 M HCOOH, (red line) 0.5 M HCOOH + 0.2 M dema, (green line) 0.5 M HCOOH + 0.5 M dema, (blue line) 0.5 M HCOOH + 0.8 M dema, and (pink line) 0.5 M HCOOH + 0.1 M TfOH.

Figure 7. Cyclic voltammograms of Ar-saturated [dema][HfB], recorded using a 50-μm diameter Pt UME at 50 mV s^{-1}. The potential was swept between −0.3 V (initial potential) and 1.4 V. The solid lines show voltammogram recorded in the absence of HCOOH, and the dashed

lines show that recorded after addition of 0.5 M HCOOH. The inset shows a magnified view of the voltammogras in the low-potential region.

Figure 8. Linear sweep voltammograms of Ar-saturated [dema][HfB] containing 0.5 M HCOOH, recorded using a 50-μm diameter Pt UME at 50 mV s^{-1}. The solid line shows the voltammogram recorded in as-synthesised [dema][HfB], and the dotted and dashed lines show those recorded in the presence of 60 mM excess HfBH, and 120 mM dema, respectively.

References

[1] R. Hayes, G. G. Warr, R. Atkin, *Chem. Rev.* **2015**, *115*, 6357-6426.

[2] M. V. Fedorov, A. A. Kornyshev, *Chem. Rev.* **2014**, *114*, 2978-3036.

[3] S. E. Goodwin, D. A. Walsh, *J. Phys. Chem. C* **2016**, *120*, 11498-11507.

[4] O. Fontaine, C. Lagrost, J. Ghilane, P. Martin, G. Trippe, C. Fave, J. C. Lacroix, P. Hapiot, H. N. Randriamahazaka, *J. Electroanal. Chem.* **2009**, *632*, 88-96.

[5] M. J. A. Shiddiky, A. A. J. Torriero, *Biosens. Bioelectron.* **2011**, *26*, 1775-1787.

[6] M. Moreno, E. Simonetti, G. B. Appetecchi, M. Carewska, M. Montanino, G.-T. Kim, N. Loeffler, S. Passerini, *J. Electrochem. Soc.* **2017**, *164*, A6026-A6031.

[7] H. M. Coromina, B. Adeniran, R. Mokaya, D. A. Walsh, *J. Mater. Chem. A* **2016**, *4*, 14586-14594.

[8] S.-Y. Lee, A. Ogawa, M. Kanno, H. Nakamoto, T. Yasuda, M. Watanabe, *J. Am. Chem. Soc.* **2010**, *132*, 9764-9773.

[9] C. A. Angell, W. Xu, M. Yoshizawa-Fujita, A. Hayashi, J. P. Belieres, P. Lucas, M. Videa, Z.-F. Zhaio, K. Ueno, Y. Ansari, J. Thomson, D. Gervasio, in *Electrochemical*

Aspects of Ionic Liquids, 2nd ed. (Ed.: H. Ohno), John Wiley & Sons, New Jersey, **2011**, p. 6.

[10] M. Yoshizawa, W. Xu, C. A. Angell, *J. Am. Chem. Soc.* **2003**, *125*, 15411-15419.

[11] D. R. MacFarlane, M. Forsyth, E. I. Izgorodina, A. P. Abbott, G. Annat, K. Fraser, *Phys. Chem. Chem. Phys.* **2009**, *11*, 4962-4967.

[12] G. L. Burrell, I. M. Burgar, F. Separovic, N. F. Dunlop, *Phys. Chem. Chem. Phys.* **2010**, *12*, 1571-1577.

[13] S. E. Goodwin, D. Smith, J. Gibson, R. G. Jones, D. A. Walsh, *Langmuir* **2017**, *33*, 8436-8446.

[14] A. M. O'Mahony, D. S. Silvester, L. Aldous, C. Hardacre, R. G. Compton, *J. Chem. Eng. Data* **2008**, *53*, 2884-2891.

[15] U. Schroder, J. D. Wadhawan, R. G. Compton, F. Marken, P. A. Z. Suarez, C. S. Consorti, R. F. de Souza, J. Dupont, *New J. Chem.* **2000**, *24*, 1009-1015.

[16] C. Zhao, G. Burrell, A. A. J. Torriero, F. Separovic, N. F. Dunlop, D. R. MacFarlane, A. M. Bond, *J. Phys. Chem. B* **2008**, *112*, 6923-6936.

[17] J. A. Bautista-Martinez, L. Tang, J. P. Belieres, R. Zeller, C. A. Angell, C. Friesen, *J. Phys. Chem. C* **2009**, *113*, 12586-12593.

[18] C. G. Zoski, *Electroanalysis* **2002**, *14*, 1041-1051.

[19] D. A. Walsh, A. Ejigu, S. Muhammad, P. Licence, *ChemElectroChem* **2014**, *1*, 281-288.

[20] C. L. Bentley, A. M. Bond, A. F. Hollenkamp, P. J. Mahon, J. Zhang, *J. Phys. Chem. C* **2014**, *118*, 29663-29673.

[21] A. Ejigu, D. A. Walsh, *J. Phys. Chem. C* **2014**, *118*, 7414-7422.

[22] Y. Meng, S. Norman, C. Hardacre, R. G. Compton, *Phys. Chem. Chem. Phys.* **2013**, *15*, 2031-2036.

[23] S. Trasatti, O. A. Petrii, *Pure Appl. Chem.* **1991**, *63*, 711-734.

[24] D. A. Walsh, K. R. J. Lovelock, P. Licence, *Chem. Soc. Rev.* **2010**, *39*, 4185-4194.

[25] P. Sun, F. O. Laforge, M. V. Mirkin, *Phys. Chem. Chem. Phys.* **2007**, *9*, 802-823.

[26] A. Berna, J. M. Feliu, L. Gancs, S. Mukerjee, *Electrochem. Commun.* **2008**, *10*, 1695-1698.

[27] W. Chen, J. Kim, S. H. Sun, S. W. Chen, *Physical Chemistry Chemical Physics* **2006**, *8*, 2779-2786.

[28] M. S. El-Deab, A. M. Mohammad, G. A. El-Nagar, B. E. El-Anadouli, *J. Phys. Chem. C* **2014**, *118*, 22457-22464.

[29] L. Johnson, A. Ejigu, P. Licence, D. A. Walsh, *J. Phys. Chem. C* **2012**, *116*, 18048-18056.

[30] A. Miki, S. Ye, M. Osawa, *Chem. Commun.* **2002**, 1500-1501.

[31] Y. X. Chen, M. Heinen, Z. Jusys, R. J. Behm, *Angew. Chem. Int. Ed.* **2006**, *45*, 981-985.

[32] J. Joo, T. Uchida, A. Cuesta, M. T. M. Koper, M. Osawa, *J. Am. Chem. Soc.* **2013**, *135*, 9991-9994.

[33] J. Joo, T. Uchida, A. Cuesta, M. T. M. Koper, M. Osawa, *Electrochimica Acta* **2014**, *129*, 127-136.

[34] K. A. Schwarz, R. Sundararaman, T. P. Moffat, T. C. Allison, *Phys. Chem. Chem. Phys.* **2015**, *17*, 20805-20813.

[35] S. Brimaud, J. Solla-Gullón, I. Weber, J. M. Feliu, R. J. Behm, *ChemElectroChem* **2014**, *1*, 1075-1083.

[36] M. S. Miran, H. Kinoshita, T. Yasuda, M. A. B. H. Susan, M. Watanabe, *Phys. Chem. Chem. Phys.* **2012**, *14*, 5178-5186.

[37] J. Stoimenovski, E. I. Izgorodina, D. R. MacFarlane, *Phys. Chem. Chem. Phys.* **2010**, *12*, 10341-10347.

[38] D. Millán, M. Rojas, J. G. Santos, J. Morales, M. Isaacs, C. Diaz, P. Pavez, *J. Phys. Chem. B* **2014**, *118*, 4412-4418.

[39] R. Barhdadi, M. Troupel, C. Comminges, M. Laurent, A. Doherty, *J. Phys. Chem. B* **2012**, *116*, 277-282.

FIGURE 1

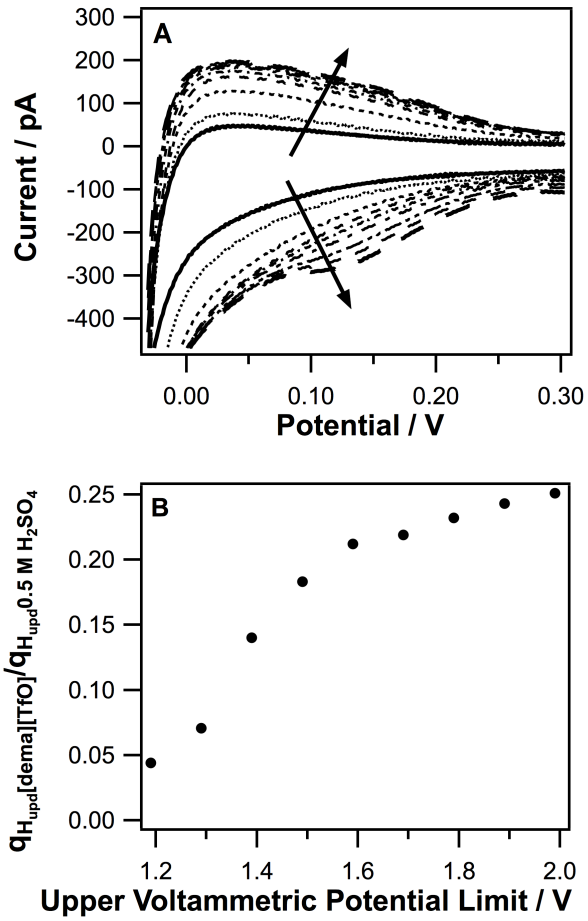
A
Current / pA
300
200
100
0
-100
-200
-300
-400
0.00
0.10
0.20
0.30
Potential / V
B
$q_{H_{upd}[dema][TfO]}/q_{H_{upd}0.5\ M\ H_2SO_4}$
0.25
0.20
0.15
0.10
0.05
0.00
1.2
1.4
1.6
1.8
2.0
Upper Voltammetric Potential Limit / V

FIGURE 2

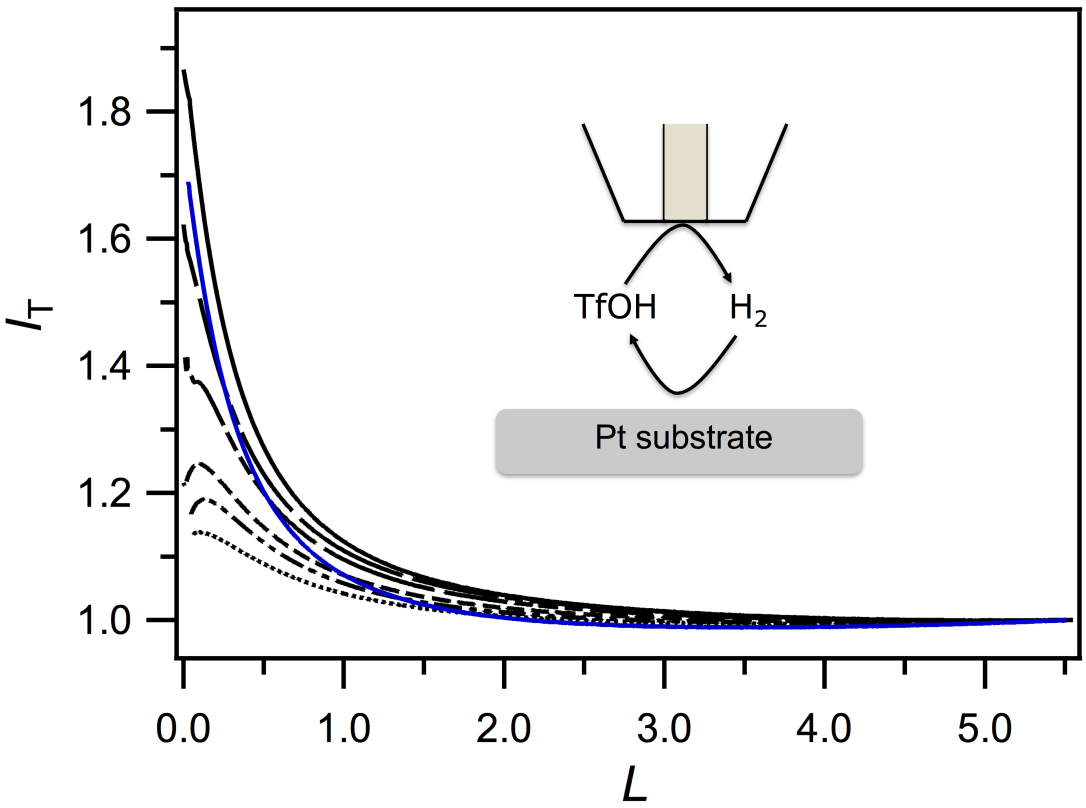

FIGURE 3

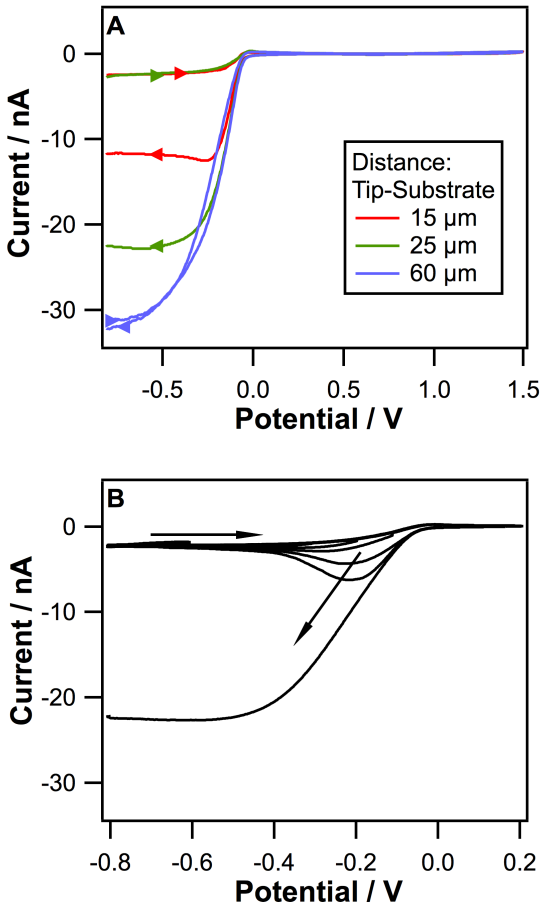
A
0
-10
-20
-30
Current / nA
-0.5
0.0
0.5
1.0
1.5
Potential / V
Distance:
Tip-Substrate
15 µm
25 µm
60 µm
B
0
-10
-20
-30
Current / nA
-0.8
-0.6
-0.4
-0.2
0.0
0.2
Potential / V

FIGURE 4

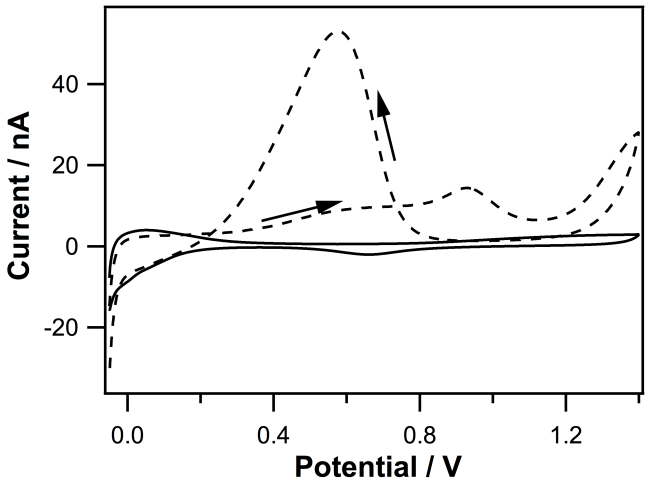

FIGURE 5

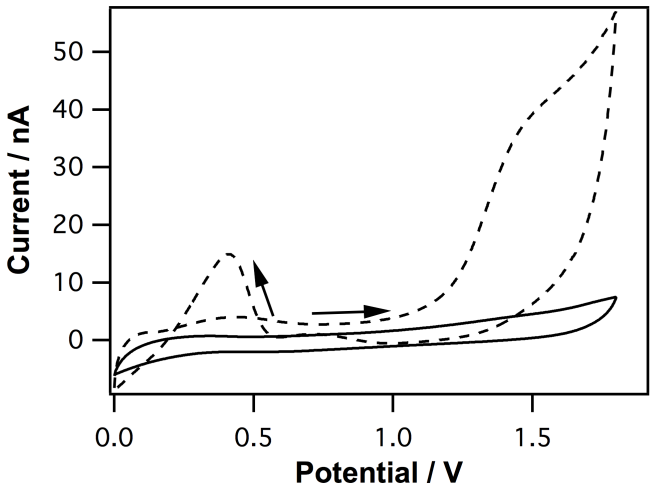

FIGURE 6

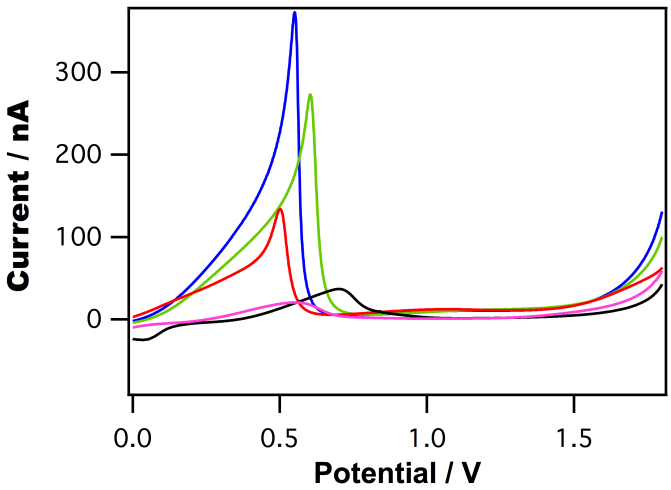

FIGURE 7

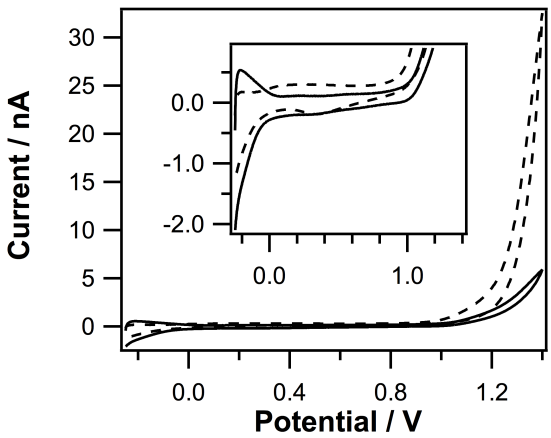

FIGURE 8